Well-defined surface tungstenocarbyne complex through the reaction of [W(C t Bu)(CH 2 t Bu) 3] with CeO 2 : a highly stable precatalyst for NOx reduction with NH 3

Cherif Larabi, Cuirong Chen, Nicolas Merle, Marc Charlin, Kai Szeto, Aimery De mallmann, Anass Benayad, Karima B. Meziane, Akim Kaddouri, Hai Nguyen, et al.

Well-Defined Surface Tungstenocarbyne complex through the Reaction of [W(≡C*t*Bu)(CH_2*t*Bu)$_3$] with CeO_2: a highly and stable precatalyst for NO_x reduction with NH_3

Cherif Larabi,[a] Cuirong Chen,[a] Nicolas Merle,[a,b] Marc O. Charlin,[a] Kai C. Szeto,[a] Aimery de Mallmann, [a] Anass Benayad,[c] Karima B. T. Meziane,[b] Akim Kaddouri,[d] Hai P. Nguyen*[e] and Mostafa Taoufik*[a]

[a] *Université Lyon 1, Institut de Chimie Lyon, CPE Lyon CNRS, UMR 5265 C2P2, LCOMS, 43 Bd du 11 Novembre 1918, 69616 Villeurbanne Cedex, France.*

[b] *Univ. Lille, CNRS, Centrale Lille, ENSCL, Univ. Artois, UMR 8181, UCCS – Unité de Catalyse et Chimie du Solide, F-59000 Lille, France*

[c] *Université Grenoble Alpes, CEA−LITEN, 17 rue des Martyrs, 38054 Grenoble Cedex 9, France*

[d] *Université Lyon 1 - CNRS, UMR 5256, IRCELYON, 2 Avenue Albert Einstein, F-69626 Villeurbanne, France*

[e] *Toyota Motor Europe, 1930 Zaventem, Belgium.*

Corresponding authors:

mostafa.taoufik@univ-lyon1.fr

Hai.P.Nguyen@toyota-europe.com

Keywords: DeNOx, Single site catalyst, Ceria, Tungsten, XAFS

Abstract

A novel well-defined precatalyst for ammonia selective catalytic reduction of NO_x (NH_3-SCR), namely [W(≡C*t*Bu)(CH_2*t*Bu)$_3$]/CeO_2 was prepared by surface organometallic chemistry and characterized. Due to the high dispersion of the active phase, this catalyst showed an excellent activity after calcination at 500°C, described by up to 99 % conversion of NO_x, high N_2 selectivity, broad operation temperature window (225 - 500 °C) and an extremely high durability for the selective catalytic reduction of NO_x with NH_3.

1. Introduction

Significant worldwide increase of stationary thermal power plants and mobile combustions engines culminates with the production of large quantity of carbon dioxide and nitrogen oxides (NO_x). NO_x contributes to ecosystem damage, serious health issues and worsens the climate changes, through the greenhouse effect, acid rains and ozone destruction.[1] Therefore, the emission level legislation of this pollutant has been drastically going down.[2,3]

The NO_x emissions were minimized through improvements such as exhaust gas recirculation, homogeneous charge compression ignition technologies and optimized injection systems as well as improved air control.[4] These reducing measures would lower the emission of NO_x albeit with the net increase of the particulate matter (PM) amount and unburned hydrocarbons. As the PM and NO_x emission are totally dependent, the declining of the former trigger the rising of the latter and vice-versa. Thus, to improve the combustion engine efficiency and minimize fuel consumption, it is desirable to operate at a lean fuel mixture, this is typically the case, for diesel engine.[5] Under these conditions, in addition to a complete combustion product (CO_2 and H_2O), a significant amount of NO_x is produced. Therefore, exhaust gas after-treatment systems are necessary in order to meet the stringent harmful emission limits. Catalysis has made impressive development in the field of NO_x reduction, since the beginning of the eighties, by the implementation of the three way catalyst systems. However, the diesel exhaust composition brings new challenges that mobilized industries, researchers and authorities to meet many improvement and innovative measures. Most effective and useful method for NO_x removal without compromising the engine performances is the selective catalytic reduction (SCR) assisted with reducing agents (NH_3 or hydrocarbon).[6,7] The most efficient approach is SCR using ammonia (NH_3-SCR), this process leads to high NO_x conversions at fairly low temperatures and in large temperature ranges.[8] Initially, this technology was set up in power plants and industrial installation for many years ago, but right now, they are extensively adopted to heavy-duty and light-duty trucks as well as to locomotives and ships.

A wide range of SCR catalysts have been developed. The most commercially viable and utilized catalysts are TiO_2 supported V_2O_5 associated to WO_3 or MoO_3 materials.[9,10] Though the catalytic activity of this class of materials are acceptable, they suffer however from lots of weaknesses such as low selectivity, narrow operation temperature range, poor deNO_x activity at low temperature and beyond all, another central environmental issue due to the releasing of deleterious and toxic VO_x species.[11] It has been a non-stop story since then, and several efficient catalysts based on transition (W, Nb, Mo, Zr, Ta,…)[12] and rare earth metals (Ce, Y,..)[13] have been well described. In particular, relevant studies on new catalytic systems as WO_3-CeO_2, Nb_2O_5-CeO_2, MnO_x-WO_3-CeO_2, Cu-Zeolite and Fe-zeolite have brought important improvement in the field of NOx reduction.[13-15] Due to the oxygen buffering capacity and redox properties of the ceria, it is widely used in these processes.[16] The major drawbacks of pure ceria relate to low thermal resistance and weak acidity. Hence, in order to improve these properties, new ceria based catalysts have been developed the use of ceria doped with other rare-earth or transition metal oxides such as ZrO_2, TiO_2 and their modification with WO_3 which improves their redox properties, thermal stability as well as surface acidity.[13,16]

Recently, through several mechanistic studies, it was found that the catalytic activity depends not only on the acidic and redox properties of the material,[9,17] but also on the metal-support interactions.[18] In particular, the nature of the supported tungsten species is determining factor. The

reported Conventional catalysts are normally prepared by uncontrolled impregnation, resulting in different species, including isolated surface tungsten sites, WxOy clusters, amorphous WO_3 and $Ce_2(WO_4)_3$.[19] Indeed, those phases are all observed by any characterization technique and this will thereby complicate the surface species identification and the drawing of structure-activity relationship.

It has been proposed that single-site heterogeneous catalysts with a controlled coordination sphere of the metal are highly effective for the selective reduction of NO_x.[20] The key step is the formation of isolated supported metal species which improves the metal dispersion, increases the metal-support interactions. Therefore, a powerful approach known as surface organometallic chemistry (SOMC) can be applied in order to prepare such single-site species. This methodology involves the controlled grafting of a suitable organometallic precursor on a support, creating a firmly bonded surface organometallic fragment. Previous studies have shown that catalytic materials prepared through this approach can lead to an enhanced activity and facilitate further mechanistic studies.[21] Moreover, great efforts have been devoted toward achieving high-performance catalysts via a chemical design. It is believed that the missing link for the use of catalysts in automotive applications is related to increasing the amount of nanosized and atomic-scale catalysts without impinging on their size, structure, shape, and interactions. This can be carefully monitored by SOMC.[22]

However commercial SCR catalysts are loaded with high amounts of WO_3,[23,24] in order to ensure a higher stability and a sufficient acidity, thus increasing the NH_3 adsorption strength which improves the activity and also the selectivity by inhibiting the oxidation of NH_3.[17] This phenomenon is also found in the case of industrial metathesis catalysts, where a high amount of metal such as tungsten, ca. 10 wt%, is required to reach high catalytic activities while only a low fraction of metal sites is active.[25] And then, based on studies that unraveled the structure of the active species,[26-28] surface organometallic chemistry has led to the development of well-defined highly active catalysts that contain only a low amount of metal. [29-33] On the other hand, surface organometallic chemistry on oxidizing support and for deNO_x applications is rare. We hereby report the first example of a highly active deNO_x catalyst with low loading prepared by the grafting a Schrock type tungsten complex on ceria along with its characterization.

2. Results and discussion

2.1. Grafting of W(≡C*t*Bu)(CH_2*t*Bu)$_3$ *on the ceria (*$CeO_{2\text{-}200}$*) surface via SOMC approach*.

SOMC methodology was not previously investigated on a ceria support for the grafting of this tungsten complex. Prior to the catalysts preparation, the ceria support (CeO_2) was characterized. The IR spectrum of ceria dehydroxylated at 200 °C pictured in Figure 1 shows four ν(O-H) vibration bands attributed to different structures of cerium hydroxyl on the surface (terminal and bridging O-H), as reported in the literature (Figure S1).[34,35] The intensity of the band at 3714 cm^{-1} associated with isolated OH groups is weak and the spectrum is rather dominated by the broad signal centered at 3630 cm^{-1} attributed to bridged hydroxyl groups. In addition a large band centered at 3527 cm^{-1} corresponds to a residual cerium oxy-hydroxide phase located within the pores.[36] To achieve the grafting and the functionalization of surface hydroxides under optimum conditions, it is desirable to know their amount. Among different quantification methods, the chemical titration using Al(iBu)$_3$ to react with a

highly reactive organometallic complex, such as $Al(iBu)_3$ has shown to be reliable.[37] This latter reacts in pentane quantitatively with surface hydroxyl groups by releasing one equivalent of isobutane per OH (Figure S2). The quantification of isobutane by GC shows that $CeO_{2\text{-}200}$ contains 0.7 mmol $OH.g^{-1}$.

The grafting reaction of $W(\equiv C\textit{t}Bu)(CH_2\textit{t}Bu)_3$ on $CeO_{2\text{-}200}$ is carried out in pentane at room temperature during 4 h. Elemental analysis of this material showed the presence of 3.3 wt% W, which correspond to *ca.* 0.18 $mmol_W.g^{-1}$. The evaluation of the amount of carbon revealed the presence of 2.16 wt% C (1.79 $mmol_C.g^{-1}$), which gives a C/W ratio of 9.95. Furthermore, a quantitative GC analysis of the gas released during the grafting process, shows the formation of 0.38 mmol of neopentane, ca. 1.9 $\textit{t}BuCH_3$ per W. This corresponds to a partial consumption of surface hydroxyls (ca. 55 % of the initial surface O-H groups). Overall, the data are consistent with the formation of bipodal surface species bearing two ligands, by a protonolysis with surface hydroxyls leading to a concomitant release of *ca.* two neopentane per tungsten atom grafted, as highlighted in Scheme 1.

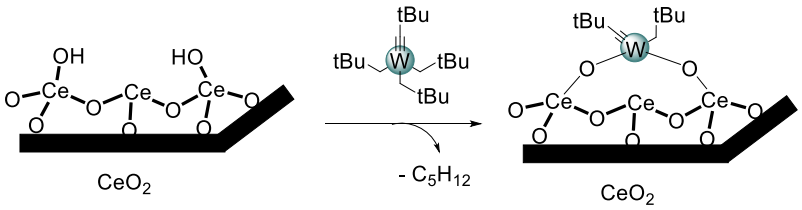

Scheme 1: Schematic illustration of the grafting of $W(\equiv C\textit{t}Bu)(CH_2\textit{t}Bu)_3$ on $CeO_{2\text{-}200}$

The textural properties of $CeO_{2\text{-}200}$ and $W(\equiv C\textit{t}Bu)(CH_2\textit{t}Bu)_3/CeO_{2\text{-}200}$ were examined by nitrogen adsorption-desorption isotherm measurements, the physisorption isotherms and the pore size distribution are depicted in Figure S3. As shown, the shape of these material isotherms correspond to type V according to IUPAC classification and display an H2-type hysteresis loop characteristic of capillary condensation between the aggregates constituting the solid. The initial increase in adsorption capacity at low relative pressure is due to monolayer adsorption. The upward deviation in the range of P/P_0 = 0.5–0.7 for the support and the catalyst is associated with progressive filling of the space between the aggregates of particles. The neat ceria has a specific surface area of ca. 205 ± 10 $m^2.g^{-1}$. It was found that the surface area was slightly decreased by a functionalization with the transition metal by reducing the value to 190 ± 10 m^2/g. The pore volumes also decreased from 0.24 ± 0.01 to 0.21 ± 0.01 $cm^3.g^{-1}$.

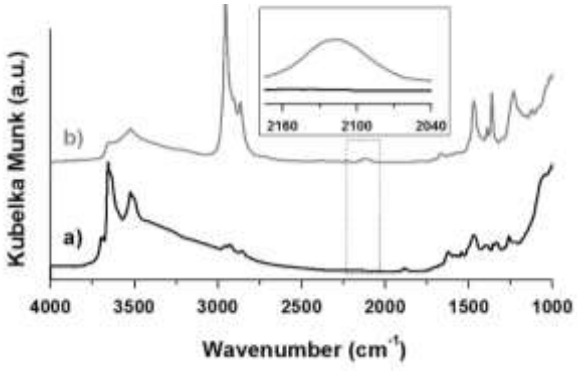

Figure 1 DRIFT spectrum of a) ceria dehydroxylated at 200 °C; b) after the grafting of $W(\equiv C\textit{t}Bu)(CH_2\textit{t}Bu)_3$.

The grafting reaction was monitored by DRIFT spectroscopy (Figure 1). After surface functionalization of ceria surface by W(≡C*t*Bu)(CH_2*t*Bu)$_3$, the isolated ν(CeO-H) band at 3712 cm^{-1} disappeared. The new bands appearing in the 3100-2850 cm^{-1} and 1620-1400 cm^{-1} ranges are characteristic of aliphatic ν(C−H), and δ(C−H) vibrations of the perhydrocarbyl ligands coordinated to surface tungsten. Noteworthy, a band at 2120 cm^{-1}, which is absent in the neat ceria sample (Figure 1a) is observed (Figure 1b). This signal has already been found and ascribed to the forbidden $2F_{5/2} \rightarrow 2F_{7/2}$ electronic transition of the subsurface Ce^{3+} (due to the partial reduction of ceria).[38] Moreover, the DRIFT spectrum of the resulting material (Figure 1b) shows a partial consumption of the other OH vibration bands, located between 3700 and 3600 cm^{-1}, while a new broad band appears, resulting from the interaction of some OH groups with tungsten alkyl ligands. The evolution of the signals in this spectral region with the grafting has already been described for the reaction of W(≡C*t*Bu)(CH_2*t*Bu)$_3$ with alumina dehydroxylated at 500 °C, where only terminal tetrahedral Al sites react completely.[39]

The X-ray diffraction analyses depicted in Figure S4, revealed that the samples exhibited the same diffraction peaks at 28.5°, 33.1°, 47.5°, 56.4°, 59.1°, 69.7° and 79.1° characteristic of the cubic fluorite structure of CeO_2.[40] This observation suggests that the functionalization did not affect the crystalline structure of ceria. From the diffraction pattern, the mean size of microcrystals could be evaluated, since it is related to diffraction peaks broadening by Scherrer's equation. The average crystal sizes thus estimated, as summarized in Table S1, indicated that the ceria particles have the tendency to agglomerate during the grafting of the tungsten complex, which corroborates the slight lowering in the surface area.

^{1}H MAS solid-state NMR spectrum of the resulting material depicted in Figure S5a, shows large signals at -3 and 0.1 ppm, tentatively attributed to the methyl of neopentyl and neopentylidyne ligands respectively. The ^{1}H NMR is less informative due to a broadening and shifting of the signal positions due to the presence of paramagnetic species (Ce^{+3}) on the catalyst.[41, 42] Moreover, from a 30% ^{13}C labelled molecular complex ^{13}C CP MAS NMR data highlighted in Figure S5b shows an intense and broad signal centered at 26 ppm assigned to the methyl of the *t*-Bu fragments and a broad, albeit weak signal at 80 ppm which can be assigned to the methylene carbons of the neopentyl fragment (-CH_2*t*Bu). A weak signal at 287 ppm can be tentatively attributed to the quaternary carbons of carbyne ligands. The broadening of the resonances and their shift to higher field is presumably due to paramagnetic Ce^{3+} ions in trigonal and cubic sites present in the ceria support as already identified.[41,42]

X-ray photoelectron spectroscopy analyses were carried out in order to provide more information on the oxidation state of the elements composing the sample: (W, Ce, O). Figure S6 shows the representative XPS spectra for the Ce 3d, O 1s and W 4f area. Generally, ten features are found in the Ce 3d region due to the pairs of spin orbit doublet as depicted in Figures S6 a and b. Six peaks are labelled v, v″, v‴ ($3d_{5/2}$) and u, u″, u‴ ($3d_{3/2}$), associated to Ce^{+4} and u^0, u', v^0, v' contribution of Ce^{+3} ($3d^{10}4f^1$), as described in the literature.[43,44] The total fraction of Ce^{3+} were estimated by taking the fitted Ce^{3+} peaks area to the total deconvoluted spectra (%Ce^{3+}= (Ce^{3+}/(Ce^{4+} + Ce^{3+}) and (%Ce^{4+}= 100 - %Ce^{3+}).[45] The concentration of Ce^{3+} in the thermally treated CeO_2 is evaluated to be ca. 32%, with respect to the total amount of Ce, thus the main oxidation state of ceria is Ce^{4+} (68%). Noteworthy, after the grafting of the organometallic complex, the amount of Ce^{3+} has slightly risen to 34%, suggesting the presence of more surface oxygen vacancies.[46] It is widely reported that concomitant presence of Ce^{3+} and Ce^{4+} offered an oxygen buffering capacity and redox properties that can promote the NO_x dissociation.[47, 48] O 1s spectra of CeO_2 and W(≡C*t*Bu)(CH_2*t*Bu)$_3$/CeO_2 are compared and

pictured in Figure S6 c and d. The peaks are quite large, leading to two binding energy contributions for O^{2-}: 531 eV and a shoulder at 532.5 eV, respectively assigned to lattice oxygen (O^{2-}) of CeO_2 (denoted O_β)[47] and to surface oxygen (denoted as O_α) such as (O^-) in defect oxide or OH,[46] respectively. The relative amounts of O_α calculated ($O_\alpha/(O_\alpha+O_\beta)$) were 45% for neat CeO_2 and 37% for $W(\equiv C\textit{t}Bu)(CH_2\textit{t}Bu)_3/CeO_{2\text{-}200}$. The partial suppression of the O_α can be attributed to their interaction with the grafted W.[19] The chemisorbed oxygen may promote the oxidation of NO to NO_2, inducing the "Fast SCR", and result in higher overall SCR catalytic activity.[49] But also can promote high temperature oxidation of NH_3 and affect the selectivity.[18] Thus, a suitable amount of O_α is desired in order to increase the reaction rate but not too much since it might affect the selectivity.[18] Thus, an optimal amount of O_α is desirable in order to increase the reaction rate by not too much since it might affect the selectivity.[50] The XPS analysis was also used to investigate the oxidation state of tungsten loaded on the support. The W4f signal is depicted in Figure S6 e, it shows the presence of two signals attributed to W $4f_{5/2}$ and $4f_{7/2}$ at 37.5 and 35.3 eV respectively, after deconvolution. These values are characteristic of W (+VI) for the grafted complex. The W4f peaks overlap with the Ce 5 s peaks, as showed in Figure S6f, making discrepancies for the curve deconvolution, nevertheless, these results are consistent with the presence of only W(+VI) but maybe with some light structure heterogeneities. Electron paramagnetic resonance (EPR) spectroscopy of the $W(\equiv CtBu)(CH2tBu)_3/CeO_{2\text{-}200}$ catalyst depicted in Figure S7 did not show any signal of isolated W(V) ions expected with g factor between 1.39 and 1.85.[51] This suggest that all tungsten atoms are present in oxidation state of W(VI).

The sample with 3.3 wt% W was studied by X-ray absorption spectroscopy (Figure 2 and Table 1), in order to shed light on the structure of the supported species.

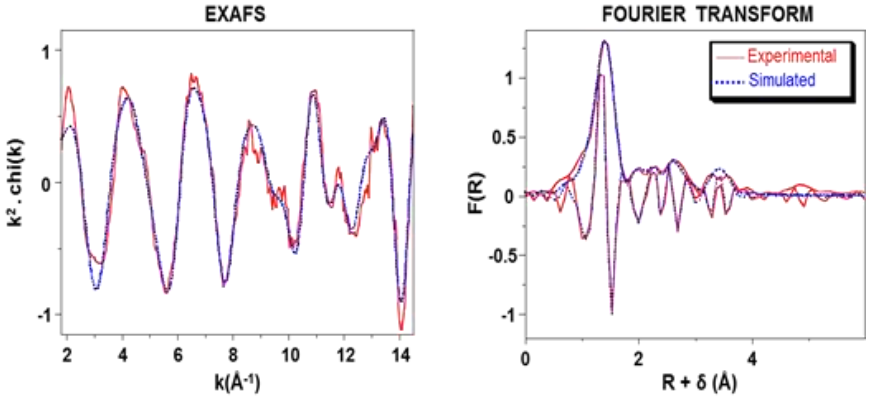

Figure 2 W LIII-edge k^2-weighted EXAFS (left) and its Fourier transform (right) for $W(\equiv C\textit{t}Bu)(CH_2\textit{t}Bu)_3/CeO_{2\text{-}200}$ material. Solid lines: experimental and dashed lines: spherical wave theory.

For the first peak of the Fourier transform (right in Figure 2), two levels of coordinated light atoms back-scatterers could be evidenced at ca. 1.78 Å and 2.26 Å. Considering the level at 1.78 Å, two types of atoms, O and C were considered, oxygen coming from the ceria surface and carbon from a carbyne ligand. The parameters thus extracted from the fit of the EXAFS signal are in agreement with a bipodal structure, $(\text{-O})_2W(\equiv C\textit{t}Bu)(CH_2\textit{t}Bu)$, with ca. two oxygen atoms at 1.78(1) Å, ca. one carbon atom at 1.78(1) Å and another one at 2.26(3) Å, attributed most probably to carbon atoms of a neopentylidyne and a neopentyl ligands respectively. The W-O distance seems marginally short but tungsten has been found to be surrounded by around six oxygen atoms at 1.787(1) Å in a $W_{0.2}Ce_{0.8}O_2$ mixed metal oxide.[52]

Table 1: EXAFS parameters for the supported complex, W(≡C*t*Bu)(CH_2*t*Bu)$_3$/CeO_2.[(a)] The errors generated by the EXAFS fitting program "RoundMidnight" are indicated between parentheses.

Type of neighbor	Number of neighbors	Distance (Å)	σ^2 (Å^2)
W≡**C**CMe_3	1.1(2)	1.78(1)	0.0011(6)
W*-*OCe	1.9(3)	1.78[(b)]	0.0011[(b)]
W*-*CH_2CMe_3	1.0(2)	2.26(3)	0.0011[(b)]
W*--*O(Ce)	1.9(5)	2.69(2)	0.0015(10)
W*--*O(Ce)	3.0(8)	2.94(3)	0.0015[(b)]
W≡C**C**Me_3	1.1[(b)]	3.25(6)	0.0015[(b)]
W*-O*Ce	1.0(4)	3.58(3)	0.0015[(b)]

[(a)] Δk: [1.8 - 14.5 Å^{-1}] - ΔR: [0.5-4.0 Å]; S_0^2 = 0.94; ΔE_0 = 4.7 ± 1.2 eV (the same for all shells); Fit residue: ρ = 5.6 %; Quality factor: $(\Delta\chi)^2/\nu$ = 2.36 (ν = 15 / 30). [(b)] Shell constrained to a parameter above.

Moreover the two carbon back-scatterers are located at distances in the range of W≡C and W-C triple and single bonds respectively, as observed in [W(≡CCMe_3)(=C$HCMe_3$)(CH_2CMe_3)(dmpe)] molecular complex (1.785(8) Å for W≡C*t*Bu and 2.258(9) Å for W-CH_2*t*Bu).[53] Similar parameters were obtained when fitting the $k^3\chi(k)$ spectrum. The fit could be also improved by adding further layers of back-scatters, with in particular two types of oxygen atoms at 2.69(2) and 2.94(2) Å and only ca. one cerium atom at 3.57(3) Å. The inclusion of tungsten as a second neighbor was not statistically validated. Therefore, this EXAFS study suggests a single-site structure ((-O)$_2$W(≡C*t*Bu)(CH_2*t*Bu)), as the one represented in Figure 3, where the tungsten atom is in a pseudo-octahedral environment can be tentatively proposed (in the cerium oxide crystal,[54] the Ce-O bond distance is ca. 2.34 Å, and the shortest Ce -- Ce distance is around 3.83 Å).

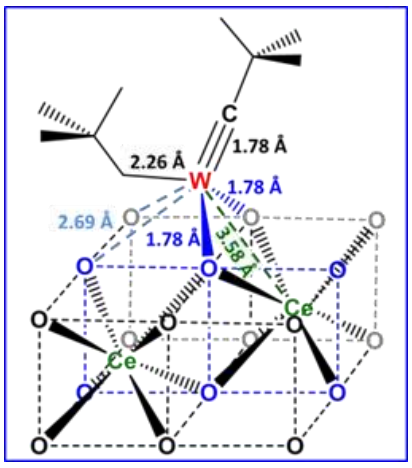

Figure 3: Proposed structure for the species resulting from the grafting of W(≡C*t*Bu)(CH_2*t*Bu)$_3$ onto $CeO_{2\text{-}200}$.

Finally, W(RCtBu)(CH2tBu)3/CeO2–200 has been submitted for HRTEM study. The distribution of atomic tungsten on the surface of ceria was confirmed in an indirect manner by HRTEM and STEM analyses (Figure S8). Indeed, the combination of HRTEM and STEM with EDX analyses showed the homogeneity of the sample. No observable cluster or nanoparticles were observed even under extensive magnification (B1 nm), but at the same time, the EDX examination confirmed the presence of W.

The reactivity of W(≡C*t*Bu)(CH_2*t*Bu)$_3$ with CeO_2 dehydroxylated at 200 °C has been investigated. The grafting occurs on Ce-OH groups by protonolysis, affording bipodal surface species, as suggested by quantification of released neopentane and elemental analysis. Further characterizations by DRIFT and solid state NMR confirm the presence of neopentyl fragments on the material. Tungsten, mainly at oxidation state VI has been revealed by XPS and EXAFS. XPS further provides quantitative information about the Ce^{3+}/Ce^{4+} ratio on the surface upon grafting. A more representative environment around tungsten on the surface is proposed by EXAFS data. Surprisingly, there is only one cerium atom being close to the tungsten center. The proposed model (Figure 3) fits well with the data and comprises bipodal tungsten surface species, as also indicated by elemental analysis.

2.2. Catalytic activity tests

The precatalyst W(≡C*t*Bu)(CH_2*t*Bu)$_3$/$CeO_{2\text{-}200}$ was calcined under dry air at 500 °C for 16 h, allowing the removal of organic ligands (Figure S9) and affording catalyst **1** before evaluating the selective reduction of NOx in a continuous flow reactor. The temperature dependencies of the NOx reduction are depicted in Figure 4. This catalyst shows more than 95 % conversion of NOx between 280 and 400 °C (Figure 4, 1st cycle). Indeed, a high activity at low temperature (200-250 °C) with a sharp increase of the conversion with temperature is observed. The selectivity for N_2 is outstandingly high until 400°C (Figure 4).

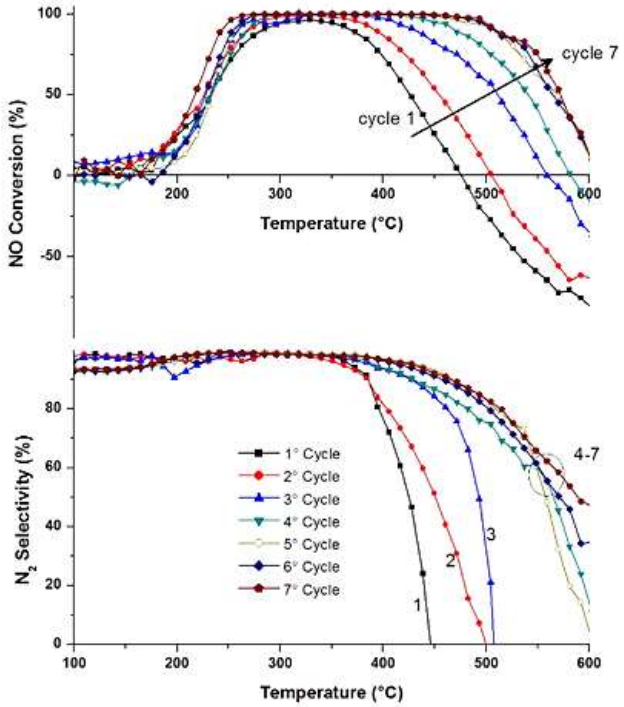

Figure 4 NO_x conversion and N_2 selectivity over **1** in function of temperature during 7 cycles. Feed composition: 300 ppm NO, 350 ppm NH_3 and 10 vol % O_2 in He.

The fresh catalyst starts to oxidize NH_3 from ca. 400 °C, resulting in a fast drop in the NO conversion and N_2 selectivity. However, upon repeating SCR cycles, we observe that the same catalyst is getting more stable, selective and temperature resistant. Full NO conversion is kept until 550 °C. Such evolution indicates that the surface sites responsible for NH_3 oxidation have been gradually inhibited. After five catalytic cycle tests, the catalyst seems to be stable and converts more than 99 % NOx between 250 and 500°C. This suggest that the surface species occur under the catalytic conditions (O_2, NH_3, NO and high temperatures) to form stable and more active species.

Moreover, long term stability of the catalyst at 300 °C was also studied. The results depicted in Figure S10 indicate that the activity of the catalysts remains stable for more than 50 h, with a conversion of ca. 99 %. To extend the behavior of this catalysts for deNOx related reactions, two experiments with a separate (NO + O_2) and (NH_3 + O_2) feed were performed. The result of NO and NH_3 oxidation versus temperature, presented in Figure S11, showed that the oxidation of NO into NO_2 occurs at low temperature, ca. 150 °C and increase linearly with the temperature to reach a pseudo-plateau between 280 and 380 °C before increasing gradually again. The first part of the curve can be explained by role of the surface oxygen available that can promote the oxidation of the NO into NO_2 to reach a plateau when the oxygen are consumed. Then thermal oxidation can follow. In contrast, the oxidation of NH_3 did not take place before the reaction temperature reaches 300 °C, where a sharp increase was observed for temperatures higher than 300 °C. This can explain the high activity observed for this SOMC catalysts where the oxidation of NO into NO_2 is favored over NH_3 oxidation, the NO_2 can promote the fast SCR.

Additional catalysis cycles have been investigated in the presence of 5 vol% water (Figure 5), reflecting more realistic conditions in combustion engines. Although the activity in the first cycle is far lower, which can be explained by the strong adsorption of water on the surface, the same tendency upon multiple recycling tests remains the same. After each catalytic run, the activity improves.

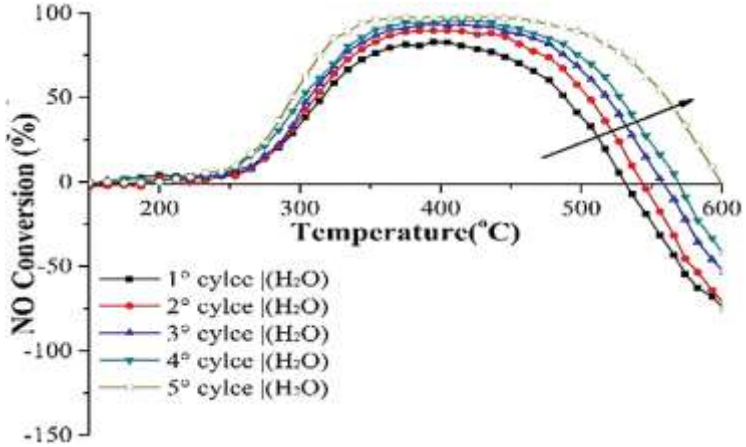

Figure 5 NOx conversion and N_2 selectivity over **1** as a function of temperature during 5 cycles. Feed composition: 300 ppm NO, 350 ppm NH_3, 5 vol% H2O, and 10 vol% O_2 in He.

This better activity is due to a better W dispersion on the ceria where only isolated sites are obtained in the case of the catalyst prepared through SOMC approach, contrary to catalysts prepared by classical methods composed of a statistical distribution of surface species (Figure S12). Thus, the catalytic behavior is highly dependent on the preparation method. The well-controlled distribution of the W species on the surface of ceria prepared through the advanced surface organometallic

functionalization could result in a higher concentration and strength of the Brønsted acids sites[19,46] or more presumably in the formation of $W_{\delta}Ce_{1-\delta}O_{2-\delta}$ clusters on the surface, highly active and more accessible to the reactants.

3. Conclusions

The present work describes the first example of a deNOx catalyst prepared by surface organometallic chemistry. The grafting of W(≡C*t*Bu)(CH_2*t*Bu)$_3$ on CeO_2 dehydroxylated at 200 °C affords isolated bipodal species, as revealed by DRIFT, solid state NMR, elemental analysis, XPS and EXAFS. The fresh catalyst transforms NO and NH_3 into N_2 in a typical exhaust gas composition after calcination at 500 °C, with almost full conversion between 280 and 400 °C. Importantly, when multiple SCR cycles were studied, the catalytic performance increased, leading to a full conversion of NO in the 220 - 500 °C temperature range, including that in the presence of 5 vol% water. Such an evolution is surprising, and is presumably due to an inhibition of NH_3 oxidation by flawed sites of ceria. The good dispersion of tungsten may also increase the acidity and oxygen-buffering capacity of the material and thereby results in a more active SCR catalyst. Ongoing experiments using in-operando techniques (EXAFS and DRIFT) during the recycling should provide information on the evolution of the catalyst when increasing the number of SCR cycles and explain the higher activity by identification of different sites on the surface.

4. Experimental section

All syntheses were performed under pure and dry argon, using a standard Schlenk techniques and a glove box. Solvents were purified and dried according to standard procedures. C_6D_6 was distilled over Na/benzophenone and stored over 3Å molecular sieves.

4.1 Characterization methods

Elemental analyses were performed at Mikroanalytisches Labor Pascher. Gas-phase analyses were performed on a Hewlett-Packard 5890 series II gas chromatograph equipped with a flame ionization detector and KCl/Al_2O_3 column (30 m × 0.32 mm). Diffuse reflectance infrared spectra were collected in a Nicolet 6700 FT-IR spectrophotometer in 4 cm^{-1} resolution. An air-tight IR cell with CaF_2 windows was applied and the final spectra comprise 64 scans. Solution NMR spectra were recorded on an Avance-300 Bruker spectrometer. All chemical shifts were measured relative to residual ^{1}H or ^{13}C resonances in the deuterated solvent: C_6D_6, δ 7.15 ppm for ^{1}H, 128 ppm for ^{13}C. ^{1}H and ^{13}C solid-state NMR spectra were recorded on Brüker Avance-500 spectrometers with a conventional double-resonance 4 mm CP-MAS probe. The samples were introduced under argon in a zirconia rotor (4 mm), which was then tightly closed. In all experiments, the rotation frequency was set to 10 kHz. Chemical shifts were given with respect to tetramethylsilane (TMS) as external reference for ^{1}H and ^{13}C NMR. X-ray diffraction was performed on a Bruker D8 diffractometer at Bragg-Bretano geometry. The instrument is equipped with Cu-tube (λ = 1.5406 Å). The Electron paramagnetic resonance (EPR) continuous-wave (CW) measurements were performed through sealed quartz tube on X-Band Bruker ELEXSYS E500 spectrometer operating at 9.8 GHz. Spectra were recorded with the same modulation frequency (100 kHz), the same modulation of amplitude and the same power level for each sample. In

order to avoid the saturation effect, the measurements were made at different microwave power levels (0.1-4 mW). The modulation of amplitude (1-5 G) was adjusted for the same reason. The low-temperature measurements were made with cryogenic systems. Specific surface area and total pore volume of the materials were measured on ASAP 2020 (Micromeritics) surface area and porosimetry system.

Extended X-ray absorption fine structure (EXAFS) spectra were acquired at ELETTRA, using XAFS beam-line (experiment code: 20145422)[55] at room temperature at the tungsten L_{III}-edge. A pair of Si(111) crystals were used as monochromator and the harmonics were rejected by a detuning of the second crystal. The spectra were recorded in the transmission mode between 9.9 and 11.43 keV. Three scans were collected for each sample. Each data set was collected simultaneously with a W metal foil reference (11206.7 eV), and was later aligned according to that reference (maximum in the first derivative of the W foil first peak). The W supported sample was packaged within a nitrogen filled glovebox in a double air-tight sample holder equipped with kapton windows. The data analyses were carried out using the program "Athena" and the EXAFS fitting program "RoundMidnight", from the "MAX" package, using spherical waves. The program FEFF8 was used to calculate theoretical files for phases and amplitudes based on model clusters of atoms. The scale factor, $S_0^2 = 0.94$, was evaluated from [W(≡CtBu)Np_3] molecular complex diluted in BN and conditioned as a pellet (one carbon at 1.76(1) Å, with three carbon atoms at 2.10(1) Å in the first coordination sphere and one carbon atom at 3.25(3) Å and three carbon atoms at 3.34(3) Å). The refinements were carried out by fitting the structural parameters N_i, R_i, σ_i and the energy shift, ΔE_0 (the same for all shells).

4.2. Materials

Ceria (CeO_2) HAS-5 Actalys 922 from Solvay ("Rare Earth La Rochelle") was calcined for 16 h at 500 °C under a flow of dry air, then evacuated under vacuum at high temperature. After a re-hydration under an inert atmosphere, the ceria was partially dehydroxylated at 200 °C under a high vacuum (10^{-5} mbar) for 15 h to give a yellow solid, noted as $CeO_{2\text{-}200}$

Tungsten complexes (W(≡CtBu)(CH_2tBu)$_3$[56], as well as 30 % labelled W(≡*CtBu)(*CH_2tBu)$_3$)[36] were prepared according to the described procedures.

4.3. Catalysts preparation

4.3.1. SOMC catalyst (**1**)

A mixture of W(≡CtBu)(CH_2tBu)$_3$ (1.6 g, 1.2 mmol) and $CeO_{2\text{-}200}$ (7 g) was stirred in pentane for 4 h, at room temperature. The W(≡CtBu)(CH_2tBu)$_3$/$CeO_{2\text{-}200}$ material was washed three times with pentane via filtration-condensation cycles. Then, all volatiles were condensed into a 6 L vessel in order to quantify neopentane evolved during the grafting reaction. After evaporation of the solvent, the resulting grey powder was dried under vacuum (10^{-5} mbar).

4.3.2. Conventional catalyst (**2**)

For comparison, the impregnated catalyst based on tungsten (W) supported on ceria was prepared by a conventional wet impregnation. In a typical reaction, at room temperature a water solution of

ammonium metatungstate ($(NH_4)_6H_2W_{12}O_{40}$, 100 mg in 5 mL of water) was added to 2 g of ceria. The suspension was stirred overnight at room temperature and then water was evacuated in a rotary evaporator at 50 °C. The material obtained was then calcined under dry air at 500 °C for 16 h. The elemental analysis indicated the presence of ca. 3.5 wt% W.

4.4. NH_3-SCR Catalytic performance tests

The NH_3-SCR catalytic evaluations were performed in a quartz fixed-bed reactor. A total gas flowrate of 300 mL.min^{-1} (hourly space velocity: 30000 h^{-1}) at atmospheric pressure, typically composed of 300 ppm NO, 350 ppm NH_3, 10 vol. % O_2 and 3 % H_2O (when used), was sent through 30 mg of $W(\equiv CtBu)(CH_2tBu)_3/CeO_{2\text{-}200}$ catalyst diluted with 500 mg of silicon carbide, in order to ensure a volume of 1 cm^3. The reactor equipped with an internal thermometer, was heated from room temperature to 600 °C with a heating rate of 10 °C.min^{-1}. The system was kept at 600 °C for 10 min before cooling down. Analyses of the gas concentrations of NO, NO_2, N_2O and NH_3 were carried out using Antaris IGS FTIR (Thermo-Fischer) equipped with a gas cell of 200 mL. N_2 selectivity was evaluated assuming that the outlet gas contains no other N-compounds than NO, NO_2, N_2O and NH_3 (Scheme 1).

$$6NO + 4NH_3 \longrightarrow 5N_2 + 6H_2O$$
$$4NO + 4NH_3 + O_2 \longrightarrow 4N_2 + 6H_2O$$
$$6NO_2 + 8NH_3 \longrightarrow 7N_2 + 12H_2O$$
$$2NO_2 + 4NH_3 + O_2 \longrightarrow 3N_2 + 6H_2O$$
$$NO + NO_2 + 2NH_3 \longrightarrow 2N_2 + 3H_2O$$

Scheme. 1: Reactions occurring during the SCR of NO_x with NH_3.

The catalytic activity and N_2 selectivity were calculated by the following equations:[19]

$$NO_{conversion}(\%) = \frac{[NO]_{in} - [NO]_{out} - [NO_2]_{out}}{[NO]_{in}} \times 100$$

$$N_{2\ selectivity}(\%) = \frac{[NH_3]_{in} + [NO]_{in} - [NO_2]_{out} - 2[N_2O]_{out} - [NH_3]_{out}}{[NH_3]_{in} + [NO]_{in}} \times 100$$

Conflict of interest

There are no conflicts to declare.

Acknowledgements

The financial support of Toyota Motor Corporation is gratefully acknowledged. CC thanks CSC (China Scholarship Council) for financial support. At ELETTRA synchrotron light source, in Basovizza, Italy, we would like to thank Luca Olivi for his help during the recording of the X-Ray absorption spectra and for the use of the glove-box.

References

[1] R.M. Doherty, M.R. Heal, F.M. O'Connor, Environ. Health 16 (2017) 33-44.
[2] M. Fiebig, A. Wiartalla, B. Holderbaum, S. Kiesow, J. Occup. Med. Toxicol. 9 (2014) 6.
[3] N. Hooftman, M. Messagie, J. Van Mierlo, T. Coosemans, Renew. Sust. Energ. Rev. 86 (2018) 1-21.
[4] S. Ramalingam, S. Rajendran, P. Ganesan, Renew. Sust. Energ. Rev. 81 (2018) 3215-3222.
[5] F.F. Pischinger, J. Eng. Gas. Turbines Power-Trans. ASME 120 (1998) 641-647.
[6] J.Q. Xu, H.L. Wang, F. Guo, C. Zhang, J.Q. Xie, RSC Adv. 9 (2019) 824-838.
[7] S.G. Zhang, B.L. Zhang, B. Liu, S.L. Sun, RSC Adv. 7 (2017) 26226-26242.
[8] W.P. Shan, H. Song, Catal. Sci. Technol. 5 (2015) 4280-4288.
[9] G. Busca, L. Lietti, G. Ramis, F. Berti, Appl. Catal. B-Environ. 18 (1998) 1-36.
[10] J.K. Lai, I.E. Wachs, ACS Catal. 8 (2018) 6537-6551.
[11] Z.G. Liu, N.A. Ottinger, C.M. Cremeens, Atmos. Environ. 104 (2015) 154-161.
[12] R. Mrad, A. Aissat, R. Cousin, D. Courcot, S. Siffert, Appl. Catal. A-Gen. 504 (2015) 542-548.
[13] J.Q. Xu, H.J. Yu, C. Zhang, F. Guo, J.Q. Xie, New J. Chem. 43 (2019) 3996-4007.
[14] M. Moliner, A. Corma, React. Chem. Eng. 4 (2019) 223-234.
[15] L. Zhang, Q.M. Wu, X.J. Meng, U. Muller, M. Feyen, D. Dai, S. Maurer, R. McGuire, A. Moini, A.N. Parvulescu, W.P. Zhang, C. Shi, T. Yokoi, X.L. Pan, X.H. Bao, H. Gies, B. Marler, D.E. De Vos, U. Kolb, F.S. Xiao, React. Chem. Eng. 4 (2019) 975-985.
[16] Z.X. Song, P. Liu, Y.M. Fu, H.P. Liu, Z.Z. Huang, H.Y. Kang, Y.L. Mao, B. Liu, Y.F. Guo, Appl. Organomet. Chem. 33 (2019) 10.
[17] G.Z. He, Z.H. Lian, Y.B. Yu, Y. Yang, K. Liu, X.Y. Shi, Z.D. Yan, W.P. Shan, H. He, Sci. Adv. 4 (2018) 8.
[18] Z. Hu, R.T. Yang, Ind. Eng. Chem. Res. 58 (2019) 10140-10153.
[19] Y. Peng, K.H. Li, J.H. Li, Appl. Catal. B-Environ. 140 (2013) 483-492.
[20] C. Paolucci, I. Khurana, A.A. Parekh, S.C. Li, A.J. Shih, H. Li, J.R. Di Iorio, J.D. Albarracin-Caballero, A. Yezerets, J.T. Miller, W.N. Delgass, F.H. Ribeiro, W.F. Schneider, R. Gounder, Science 357 (2017) 898-+.
[21] N. Popoff, E. Mazoyer, J. Pelletier, R.M. Gauvin, M. Taoufik, Chem. Soc. Rev. 42 (2013) 9035-9054.
[22] A. Beniya and S. Higashi, Towards dense single-atom catalysts for future automotive applications, Nat. Catal., 2 (2019), 590–602.
[23] F. Can, X. Courtois, S. Berland, M. Seneque, S. Royer, D. Duprez, Catal. Today 257 (2015) 41-50.
[24] Y. Xu, X. Wu, L. Cao, Y. Ma, R. Ran, Z. Si, D. Weng, Z. Ma, B. Wang, J. Catal. 375 (2019) 294-303.
[25] S. Lwin, Y.Y. Li, A.I. Frenkel, I.E. Wachs, ACS Catal. 6 (2016) 3061-3071.
[26] A.G. Basrur, S.R. Patwardhan, S.N. Vyas, J. Catal. 127 (1991) 86-95.
[27] C. Martin, P. Malet, G. Solana, V. Rives, J. Phys. Chem. B 102 (1998) 2759-2768.
[28] A.J. van Roosmalen, D. Koster, J.C. Mol, J. Phys. Chem. 84 (1980) 3075-3079.
[29] C. Larabi, N. Merle, F. Le Quemener, P. Rouge, E. Berrier, R.M. Gauvin, E. Le Roux, A. de Mallmann, K.C. Szeto, M. Taoufik, Catal. Commun. 108 (2018) 51-54.
[30] C. Larabi, K.C. Szeto, Y. Bouhoute, M.O. Charlin, N. Merle, A. De Mallmann, R.M. Gauvin, L. Delevoye, M. Taoufik, Macromol. Rapid Commun. 37 (2016) 1832-1836.
[31] N. Merle, F. Le Quemener, S. Barman, M.K. Samantaray, K.C. Szeto, A. De Mallmann, M. Taoufik, J.M. Basset, Chem. Commun. 53 (2017) 11338-11341.
[32] N. Merle, F. Le Quemener, Y. Bouhoute, K.C. Szeto, A. De Mallmann, S. Barman, M.K. Samantaray, L. Delevoye, R.M. Gauvin, M. Taoufik, J.M. Basset, J. Am. Chem. Soc. 139 (2017) 2144-2147.
[33] F. Zhang, K.C. Szeto, M. Taoufik, L. Delevoye, R.M. Gauvin, S.L. Scott, J. Am. Chem. Soc. 140 (2018) 13854-13868.

[34] A. Badri, C. Binet, J.C. Lavalley, J. Chem. Soc.-Faraday Trans. 92 (1996) 4669-4673.
[35] B. Beck, M. Harth, N.G. Hamilton, C. Carrero, J.J. Uhlrich, A. Trunschke, S. Shaikhutdinov, H. Schubert, H.J. Freund, R. Schlogl, J. Sauer, R. Schomacker, J. Catal. 296 (2012) 120-131.
[36] M. Taoufik, E. Le Roux, J. Thivolle-Cazat, C. Coperet, J.M. Basset, B. Maunders, G.J. Sunley, Top. Catal. 40 (2006) 65-70.
[37] E. Mazoyer, J. Trebosc, A. Baudouin, O. Boyron, J. Pelletier, J.M. Basset, M.J. Vitorino, C.P. Nicholas, R.M. Gauvin, M. Taoufik, L. Delevoye, Angew. Chem.-Int. Edit. 49 (2010) 9854-9858.
[38] C. Binet, A. Badri, J.C. Lavalley, J. Phys. Chem. 98 (1994) 6392-6398.
[39] J. Joubert, F. Delbecq, P. Sautet, E. Le Roux, M. Taoufik, C. Thieuleux, F. Blanc, C. Coperet, J. Thivolle-Cazat, J.M. Basset, J. Am. Chem. Soc. 128 (2006) 9157-9169.
[40] S.A. Ansari, M.M. Khan, M.O. Ansari, S. Kalathil, J. Lee, M.H. Cho, RSC Adv. 4 (2014) 16782-16791.
[41] R.M. Rakhmatullin, V.V. Pavlov, V.V. Semashko, Phys. Status Solidi B-Basic Solid State Phys. 253 (2016) 499-503.
[42] R.M. Rakhmatullin, V.V. Semashko, S.L. Korableva, A.G. Kiiamov, A.A. Rodionov, R. Tschaggelar, J.A. van Bokhoven, C. Paun, Mater. Chem. Phys. 219 (2018) 251-257.
[43] C. Anandan, P. Bera, Appl. Surf. Sci. 283 (2013) 297-303.
[44] Y. Zhu, N. Jain, M.K. Hudait, D. Maurya, R. Varghese, S. Priya, J. Vac. Sci. Technol. B 32 (2014) 11.
[45] X.J. Yao, Z. Wang, S.H. Yu, F.M. Yang, L. Dong, Appl. Catal. A-Gen. 542 (2017) 282-288.
[46] W.P. Shan, F.D. Liu, H. He, X.Y. Shi, C.B. Zhang, Appl. Catal. B-Environ. 115 (2012) 100-106.
[47] X.S. Dong, J.H. Wang, H.W. Zhao, Y.D. Li, Catal. Today 258 (2015) 28-34.
[48] X.J. Yao, T.T. Kong, L. Chen, S.M. Ding, F.M. Yang, L. Dong, Appl. Surf. Sci. 420 (2017) 407-415.
[49] H.D. Xu, M.M. Sun, S. Liu, Y.S. Li, J.L. Wang, Y.Q. Chen, RSC Adv. 7 (2017) 24177-24187.
[50] S. Liu, R. Zhang, P. Li, H. Chen, Y. Wei, X. Liang, Catal. Today 339 (2020) 241-253. DOI:10.1016/j.cattod.2019.1002.1004.
[51] S. Kuba, P.C. Heydorn, R.K. Grasselli, B.C. Gates, M. Che, H. Knozinger, Phys. Chem. Chem. Phys. 3 (2001) 146-154.
[52] Z.Y. Liu, W.Q. Xu, S.Y. Yao, A.C. Johnson-Peck, F.Z. Zhao, P. Michorczyk, A. Kubacka, E.A. Stach, M. Fernandez-Garcia, S.D. Senanayake, J.A. Rodriguez, J. Catal. 321 (2015) 90-99.
[53] M.R. Churchill, W.J. Youngs, Inorg. Chem. 18 (1979) 2454-2458.
[54] E.A. Kummerle, G. Heger, J. Solid State Chem. 147 (1999) 485-500.
[55] A. Di Cicco, G. Aquilanti, M. Minicucci, E. Principi, N. Novello, A. Cognigni, L. Olivi, 14th International Conference on X-Ray Absorption Fine Structure, Iop Publishing Ltd, Bristol.
[56] D.N. Clark, R.R. Schrock, J. Am. Chem. Soc. 100 (1978) 6774-6776.